Diamond & Related Materials 109 (2020) 108020

Contents lists available at ScienceDirect

Diamond & Related Materials

journal homepage: www.elsevier.com/locate/diamond

Anomalous behaviour of surface Brillouin scattering in thin strained CVD diamond

I. Motochi[a,*], B.A. Mathe[b], S.R. Naidoo[b], E. Aradi[c]

[a] Dept of Mathematics and Physical Sciences, Maasai Mara University, P.O Box 861-20500, Narok, Kenya
[b] Materials Research Institute, DST-NRF Centre of Excellence in Strong Materials and School of Physics, University of the Witwatersrand, Wits 2050, Johannesburg, South Africa
[c] School of Computing and Engineering, University of Huddersfield, Queensgate, Huddersfield HD1 3DH, United Kingdom

ARTICLE INFO

Keywords:
Diamond
Surface Brillouin scattering
Recrystallization
Graphite
Wipe out
Ion implantation

ABSTRACT

Hellium ions were implanted into diamond at energies of 80 and 160 keV with fluences beyond the amorphization threshold using the Cold Implantation Rapid Annealing (CIRA) technique. A thin recrystallized diamond layer of ≈63 nm and ≈103 nm for implantation at 80 keV and 160 keV, respectively was estimated using the constant angle reflection interference spectroscopy. Analysis on this thin diamond-graphitic carbon-bulk diamond structure was carried out using Raman spectroscopy, diffuse reflectance spectroscopy and surface Brillouin scattering. Raman analysis shows that the damaged buried layer consists of an amorphous graphitic material while the diffuse reflectance measurements showed high reflectance at the diamond-graphitic layer interface. This led to multiple reflectivity resulting in reduction of the intensity of the incident beam to ≈0.37 that gets reflected. Surface Brillouin scattering showed a weak longitudinal peak, L_{KB2} at 61.6 GHz for the recrystallized diamond layer while for the unimplanted diamond a similar peak was observed at 64.2 GHz for laser beam $\lambda = 514.5$ incident at $\theta_i = 70^{\circ}$ to the sample surface's normal. Further, surface Brillouin scattering showed an un-usual behaviour where the L_{KB2} peak disappeared after some time of collection. This was attributed to 'wipe out' phenomenon where multiple reflections resulted in multiple inelastically scattered light being detected in the recrystallized layer.

1. Introduction

Ion implantation causes stresses and strains in the implanted region of a crystalline material due to the breaking of bonds along the damage cascade caused by the implanted ions by electronic and nuclear stopping processes. Healing of the stressed/strained material is achieved by moving the target displaced atoms and implanted ion species to sites where the material attains minimum energy [1]. This is accomplished through post implantation thermal annealing. During annealing sufficient thermal energy is provided in order to recover the crystal structure of the material which was damaged in the collision cascades within the implanted region provided the defect density is not too high.

Diamond, with an electronic configuration sp^3 tends to form sp^2 carbon during irradiation once a critical radiation damage is exceeded. For moderate keV implantation energies, typically used in semiconductor doping, the simulated threshold damage density as obtained from Stopping and Range of Ions in Matter (SRIM) is $\approx 5 - 9 \times 10^{22}$ vac/cm^3 [2]. Other scientists, using 1 MeV energies found the threshold for amorphization in diamond to be $\approx 6 \pm 2 \times 10^{22}$ vac/cm^3 [3]. Upon annealing, implanted diamond remains as an amorphous sp^2/sp^3 matrix unlike other covalently bonded semiconductors Si and Ge that undergoes solid phase epitaxial regrowth [4]. It has been observed that for implantation above the critical damage density, the damaged layer graphitizes upon annealing and forms sharp boundaries with the diamond [5]. In a CIRA study using carbon ions and multiple energies, and for a total fluence above the critical damage density, a uniformly damaged graphitic layer from the surface to a depth of ≈0.25 μm was created [6] and in that work we were able to obtain the elastic properties of the amorphous carbon layer that was on top of the bulk diamond. This work sought to find out if a Rayleigh wave could be detected from the diamond layer above the graphitic layer. This was done by reducing the scattering volume to a level where the bulk modes T_{KB2} and L_{KB2} can just be observed in the thin diamond layer above the opaque amorphous layer. When this is achieved, the thin diamond layer can then be implanted with say carbon ions and the elastic properties of this layer could be studied using SBS as a function of ion fluence and

* Corresponding author.
E-mail address: Motochi@mmarau.ac.ke (I. Motochi).

https://doi.org/10.1016/j.diamond.2020.108020
Received 15 January 2020; Received in revised form 26 July 2020; Accepted 29 July 2020
Available online 07 August 2020

annealing temperature below the damage threshold that causes graphitization.

In our previous work [6], one of the studies created a buried amorphous layer of ≈50 nm of recrystallized diamond on top of an amorphous carbon. In the work described in [6] the carbon ion-implanted diamond was annealed from 600 to 1200 °C and the changes were elucidated as observed by Raman spectroscopy (RS), surface Brillouin scattering (SBS), high resolution transmission electron microscopy (HRTEM), electron energy loss spectroscopy (EELS). In this paper we investigate SBS effects where the scattering volume of the undamaged diamond cap at the surface has been increased by implanting a lighter ion at a higher energy so that the implanted fluence generates an amorphous carbon layer deeper below the diamond surface.

2. Experimental

Four CVD diamond samples purchased from Element Six Company, UK, were He^+ implanted. Two of the diamond samples had one side (P1) unpolished while the other two were polished on both sides (P2). One P1 and one P2 was implanted with 80 keV He^+ and the remaining two samples was implanted at 160 keV He^+. The P1 samples were implanted at liquid nitrogen temperature while the P2's at room temperature. The same fluence of 6×10^{16} ions/cm^2 was implanted in the four samples. The two samples implanted at liquid nitrogen were transferred from the cold stage end station target holder of the implanter into a liquid nitrogen bath and dropped into a preheated RF furnace at 1200 °C in flowing argon gas. This process is called Cold Implantation Rapid Annealing (CIRA) was developed by Prins to dope diamond [7]. The 2 samples implanted at RT were also annealed at 1200 °C in flowing argon. The anneal time was one hour for each sample. The implantation procedure was similar to that explained in the experimental section of the paper by Motochi *et al* [6]. However, the furnace used for annealing was described in [8]. The resultant sample after this process may be schematically visualized as shown in Fig. 1.

After annealing, the damage was investigated using Raman spectroscopy. Reflectivity studies using UV-VIS-NIR 500 Cary spectrophotometer was done to observe interference effects above the damaged region. Brillouin surface scattering was done to study surface acoustic waves in the thin film.

3. Results and discussion

3.1. Stopping and range of ions in matter (SRIM) simulation of he^+ implanted in diamond

A SRIM monte Carlo simulation for He^+ implanted in diamond is shown in Fig. 2. The fluence of 6×10^{16} ions/cm^2 used in this work creates a simulated damage profile where the TRIM damage density (D_c) is above and below TRIM damage density threshold of (4×10^{22} ions/cm^3) [9,10] for helium ions in diamond. This implantation would result in a relatively undamaged near surface region. The region below D_c reconstruct by recombination of vacancies and interstials and not by solid state epitaxial growth from the boundary outwards, this explains the formation of sharp boundaries at the interfaces between the top

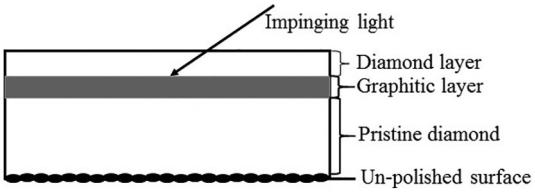

Fig. 1. Cross-section of the He ion implanted diamond after annealing (not drawn to scale).

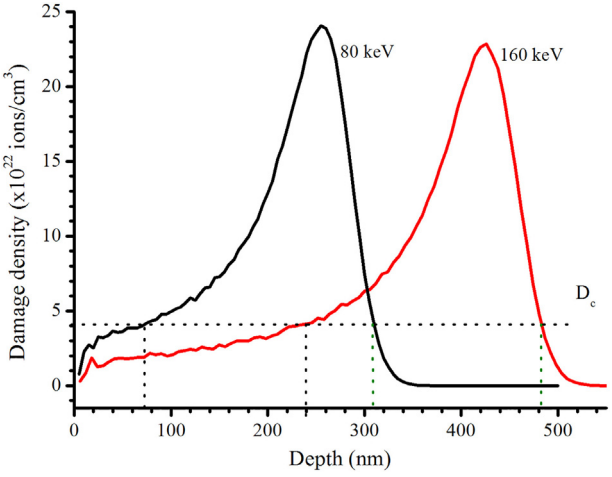

Fig. 2. TRIM simulation for 80 keV and 160 KeV He^+ energies used in implantation in diamond.

layer, the amorphous carbon layer and the virgin diamond beyond the implantation region. The top region retains the diamond structure after annealing as the damage density within this volume is below the critical damage density thus resulting in a thin layer of diamond sitting on an opaque layer of amorphous carbon and beyond the amorphous layer is the diamond substrate which was not affected by the ions.

As predicted by SRIM simulation, the He^+ implanted and annealed system is a thin transparent recrystallized diamond film ≈79 nm for 80 keV and 234 nm for 160 keV on an opaque amorphized layer of thickness 231 nm and 250 nm for energies 80 keV and 160 keV, respectively. The amorphous layer with a sharp boundary at the end of range sits on pristine diamond at ≈310 nm and ≈484 nm for the 80 keV and 160 keV implants, respectively (see Fig. 2).

3.2. Raman spectroscopy observations

The T64000 Raman spectrometer using single line modes of 514.5 nm and 785 nm was used in measurements on the He ion implanted and annealed diamond samples. The measurement show the presence of two broad bands after annealing at 1200 °C. The D peak usually centered around 1350 cm^{-1} is convoluted under a broad band that extends from 1100 to 1500 cm^{-1}. A range of Gaussian curves was used to fit the shape of the recorded Raman spectra. The fit centered around the G band is more defined and lies between 1603 and 1605 cm^{-1} for both 514.5 and 785 nm light beams. There is therefore no dispersion in the G peak which implies that the opaque implanted layer has some graphitic order. This kind of spectra is indicative of the nature of an amorphous carbon layer and peaks around 1340–1350 are due to the D peak, while peaks around 1550–1650 is related to the G peak [11].

The presence of a broad D peak implies disorder in the ion damaged region. However, a first order diamond peak was observed from the strained recrystallized diamond layer from the surface (≈ 79 nm for the 80 keV implanted diamond) that remained intact after annealing because the damage density was below the critical density for amorphization. The first order diamond signal was observed around 1326/1327 cm^{-1} using the 514.5 nm light in Fig. 3a and b implying that the diamond is under tensile stress [12]. The diamond line is not apparent in the 785 nm spectra since the red light is more sensitive to non-diamond phases.

3.3. Transmission and diffuse reflectivity measurements

The transmission spectra for P2 an unimplanted and as-implanted diamonds are shown in Fig. 4. Pure diamond transmitted ≈ 70% while

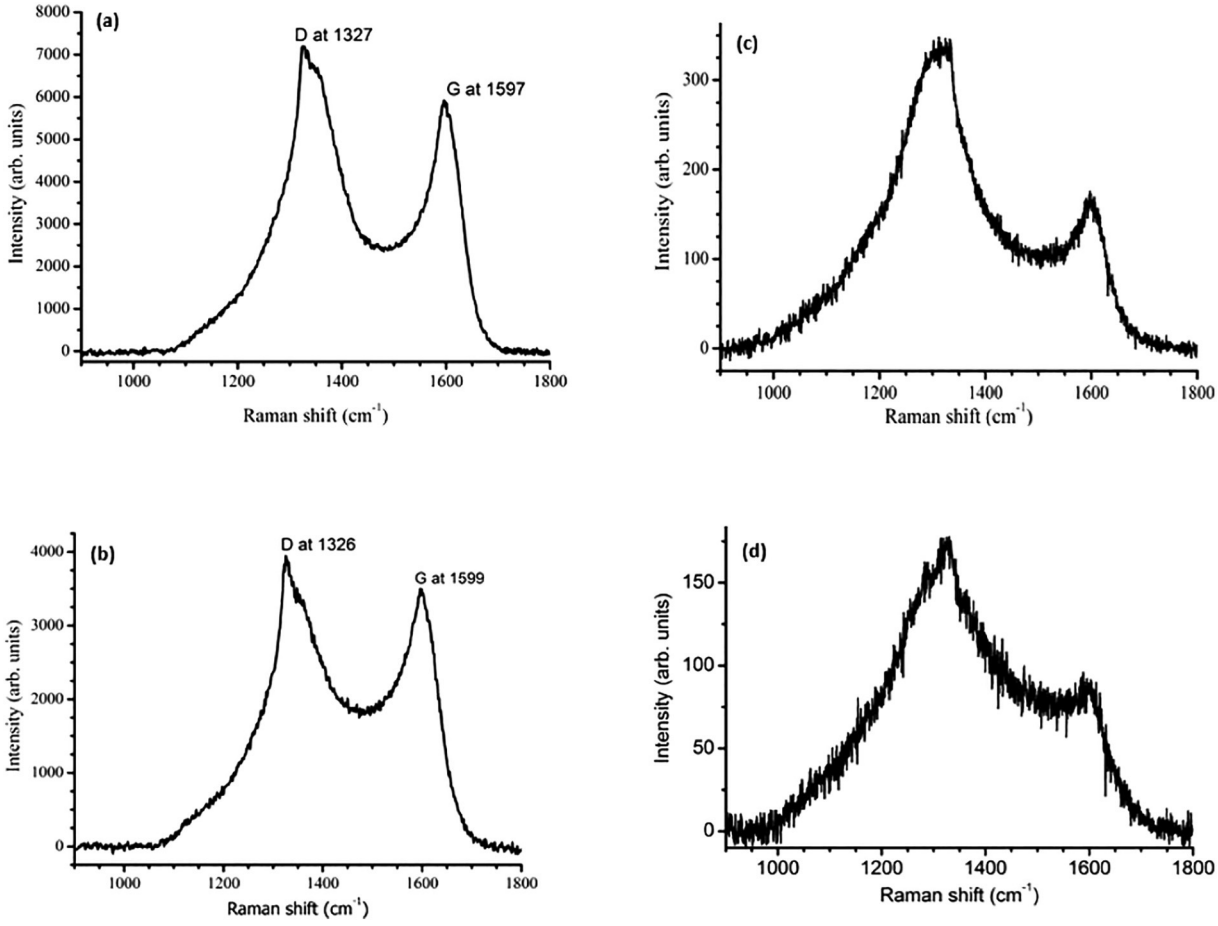

Fig. 3. Raman spectra of the P1 He ion implanted diamond after annealing 1200 °C. Figures (a) and (c) were implanted at 160 keV while (b) and (d) were implanted at 80 keV. Light of wavelength 514.5 nm was used to produce spectra (a) and (b) while that of wavelength 785 nm produced (c) and (d).

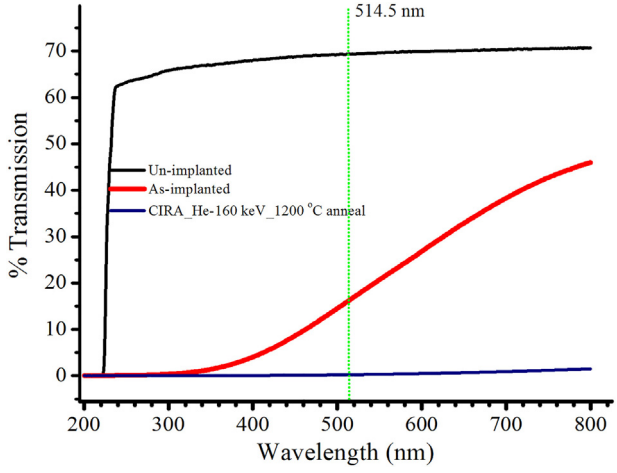

Fig. 4. Transmission spectra in the visible light range of un-implanted CVD diamond, After it is implanted with He^+ at a fluence of 6×10^{16} ions/cm^2 and the same sample after annealing at 1200 °C. There is no transmission below 220 nm, the absorption edge of diamond.

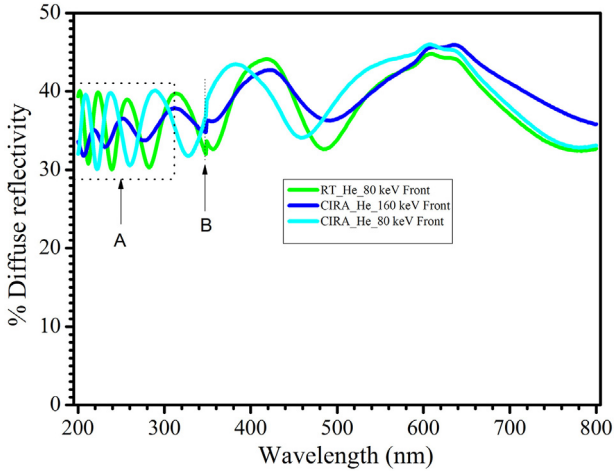

Fig. 5. Diffuse reflectance measurements on the P2 samples and one P1 samples, front means the implanted side, RT is room temperature implanted while CIRA were implanted at liquid nitrogen temperature. Analysis of wavelength and amplitudes were done in the section labelled A. The line B is an instrumental artefact.

the as-implanted transmitted ≈ 62% in the visible range. Transmission measurements conducted on all the samples after implantation and annealing show a less than 0.3% transmission of 514.5 nm light. This implies that the damaged region becomes opaque after annealing.

Constant angle reflection interference spectroscopy (CATIS) measurements in the visible range was conducted to determine the presence of a thin transparent medium sitting on an opaque surface. Fig. 5 shows the diffuse reflectivity graphs of different surfaces measured using the UV-VIS-NIR 500 Cary spectrophotometer. It was observed that those surfaces with thin transparent diamond on an opaque graphitic layer (He-ion implanted samples) resulted in a sine-like curve [13] due to

interference of waves reflected from the surface and the opaque surface at the first boundary of the diamond/opaque interface.

The 'wavelength' of the sine curve reduced with the wavelength of the light. The wavelength and amplitude of the 80 keV implanted diamonds were relatively the same for the same interval change. The amplitude of 160 keV implanted was smaller than the 80 keV implanted diamonds by 49.4%. Thick samples like pristine diamond or measurements done at the back of the amorphous layer for P2 samples do not show any interference fringes. This is attributed to the fact that the width between the end of range of ions and the back surface (region labelled 'pristine diamond' in Fig. 1) was infinitely large compared to the wavelength of light to show any interference phenomena.

The thickness of the cap layer was estimated from the period of the interference pattern at normal incidence using [14]:

$$d_k = \left| \frac{1}{2\eta\left(\frac{1}{\lambda_i} - \frac{1}{\lambda_j}\right)} \right| \tag{1}$$

where d_k is the layer thickness, η is the refractive index of the diamond, and $\lambda_{i,j}$ are the wavelengths corresponding to two consecutive maxima (or minima) in the interference pattern. The maxima and minima values of the curves are shown in Table 1.

The incident radiation normal to the surface changes from near infrared to UV. Eq. (1) is modified to account for the continuously changing wavelength of the incident radiation to:

$$d_{k1} = \frac{1}{2\eta\left(\frac{1}{\lambda_3} - \frac{1}{\lambda_2}\right)} - \frac{1}{2\eta\left(\frac{1}{\lambda_2} - \frac{1}{\lambda_1}\right)} \tag{2}$$

The average from the trough and crests of the same curve gives the estimated cap thickness, thus:

$$d = \frac{1}{4\eta}\left[\frac{1}{\left(\frac{1}{\lambda_3} - \frac{1}{\lambda_2}\right)} - \frac{1}{\left(\frac{1}{\lambda_2} - \frac{1}{\lambda_1}\right)}\right] \tag{3}$$

Taking the refractive index of diamond as 2.5 around the 300 nm value [15] and using Eq. (3), the estimated thickness of the recrystalized diamond cap were ≈58 nm, 63 nm for the room temperature and CIRA helium implanted at 80 keV, respectively. For the CIRA, 160 keV implanted diamond, the cap thickness was calculated to be ≈103 nm. These values differ from those theoretically calculated from SRIM. It is likely that the critical damage density is lower for implanted layers that are close to the diamond surface. It has been observed that for high energies ¿1 MeV, the critical damage density to achieve amorphization is higher [3].

3.3.1. Reflection from diamond surface and buried graphitic layer

As predicted by the TRIM simulation, (Fig. 2) and confirmed by calculations in Section 3.3, helium implantation at single energy resulted in a damaged layer buried beneath a diamond layer after annealing at 1200 °C. The interface of the undamaged diamond cap and buried thin film of graphitic carbon forms a mirror-like surface with a reflective surface.

Table 1
Trough and crest positions from interference pattern observed on thin diamond cap after annealing He ion implanted diamond.

Implantation environment	Implantation energy (keV)	Feature	Peak position (nm)		
			1	2	3
Room temp.	80	Trough	283	239	212
		Crest	313	257	223
CIRA	80	Trough	328	260	222
		Crest	289	238	209
	160	Trough	278	231	207
		Crest	311	252	220

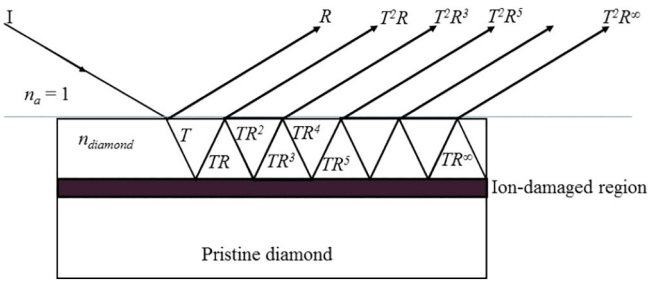

Fig. 6. Multiple reflection of light on the thin diamond film sitting on He ion damaged region.

When light is incident onto the top surface of the diamond cap, the incident ray is partly reflected and partly transmitted as refracted light. The transmitted ray, upon arrival at the interface gets partly reflected towards the surface while some fraction of it is absorbed. At the 'top' surface, some light is transmitted while some gets reflected back towards the interface. The transmitted light moves in the same direction as that initially reflected from the incident light, though with a longer pathlength. The reflected light repeats the process leading to multiple reflections. The intensity of the multiple reflections reduces after each refection. This process goes on until the light reaches the edge of the diamond film as shown in Fig. 6.

No light goes through the amorphized layer but even if some were to go through, it would be diffusely reflected at the unpolished surface and needs no further analysis.

The intensity of the reflected beam can thus be calculated from Fresnel's equations. Reflecting power or reflection coefficient (R) is the ratio of the reflected to incident intensity [16].

The complex refractive index $n = n_r(1 - i\chi)$.

for $\chi = 1$

$$R = \frac{(n_r - 1)^2 + n_r^2}{(n_r + 1)^2 + n_r^2} = \frac{2n_r^2 - 2n_r + 1}{2n_r^2 + 2n_r + 1} = \frac{1 - 1/n_r}{1 + 1/n_r} \approx 1 - \frac{2}{n_r} \tag{4}$$

For a non-transmitting medium, absorption (A) = 1-R

$$A = 1 - R = \frac{4n_r}{2n_r^2 + 2n_r + 1} \approx \frac{2}{n_r} \tag{5}$$

If the He^+ implanted layer is more graphitic after annealing then from [17], the refractive index for 500 nm light at room temperature is ≈2.6, hence; $R = 0.23$ and $A = 0.77$.

$$R = \frac{(n-1)^2}{(n+1)^2} \Rightarrow \frac{\left(\frac{n_2}{n_1} - 1\right)^2}{\left(\frac{n_2}{n_1} + 1\right)^2} = \frac{(n_2 - n_1)^2}{(n_2 + n_1)^2} \tag{6}$$

For light incident from air or vacuum, $n_2 \to 1$, and letting $n_1 \to n$, the refractive index of diamond.

$$R = \left(\frac{1-n}{1+n}\right)^2 \tag{7}$$

$R_{1\to n} = R_{n\to 1}$, similarly $T_{1\to n} = T_{n\to 1}$.

Supposing the medium does 'not absorb' any light then $T = (1 - R)$.

The total reflectance is therefore,

$$R_{Total} = R + T^2R + T^2R^3 + T^2R^5 + \cdots + T^2R^{\infty}$$

$$= R + T^2R\{1 + R^2 + R^4 \cdots + R^{\infty - 1}\}$$

$$= R + (1 - R)^2R\{1 + R^2 + R^4 \cdots + R^{\infty}\}$$

Expanding the series in {} brackets we obtain the total reflectivity.

$$R_{Total} = R + \frac{(1-R)^2R}{1-R^2} = \frac{2R - 2R^2}{1 - R^2} = \frac{2R(1-R)}{(1-R)(1+R)} = \frac{2R}{1+R} \tag{8}$$

For $R = 0.23$, then $R_{Total} = 0.37$ of the intensity of incident beam. This implies that light intensity that reaches the detector is very small hence the long time required to collect spectra.

3.4. Surface Brillouin scattering results

The He ion implanted and annealed system was a thin transparent diamond film ≈63 nm for 80 keV and 103 nm for 160 keV, CIRA treated samples as calculated from Eq. (3). This work sought to investigate the surface Brillouin acoustic modes in the recrystalized diamond cap sitting on the amorphous carbon. The amorphous layer which has a sharp boundary at end of range sits on pristine diamond. The top diamond layer on the amorphized layer is basically an optically hard material on a soft one. The expected behaviour of such a system for opaque samples is the observation of a Rayleigh mode of the top layer only [18]. However, the transparent nature of the thin diamond film therefore means the scattering volume and film-substrate interface properties has the potential to alter the outcome.

SBS measurements were done on P1 samples. The amorphous layer is opaque with a transmission of less than 0.25% hence there is no transmission through it. However, If some light passes through the layer, there can be no spectrum obtained from the unpolished surface due to diffuse scattering and any light specularly reflected back ends up being completely absorbed in the layer. The experimental setup using P1 samples of Fig. 6 therefore guarantees no light from the back of the layer. The spectra observed to be emanating from indirect scattering must be from the diamond sitting on top of the graphitic layer which was found to have reflective properties (see Section 3.3). The scattering geometry which applies for transparent sample shown in Fig. 7 was employed for analysis [19].

Measurements involving an extended free spectral range (FSR) produced L_{KB1} after a very long collection time as expected due to the limited scattering volume of the top thin diamond layer. The longitudinal peak L_{KB1} at ≈42 GHz due to direct scattering was therefore from strained diamond sitting on the opaque layer, for laser beam $\lambda = 514.5$ incident at $\theta_i = 70°$ to the sample surface's normal [19].

Weak peaks were observed in positions L_{KB2} and T_{KB2} using p-polarized and s-polarized light, respectively. These peaks would however disappear (a phenomenon we called 'wipe out') as measurements progressed. The indirectly scattered L_{KB2} peak observed after close to 4 h seems to have been completely wiped out after 20 h but seems to be growing again after 34 h as seen in Fig. 8.

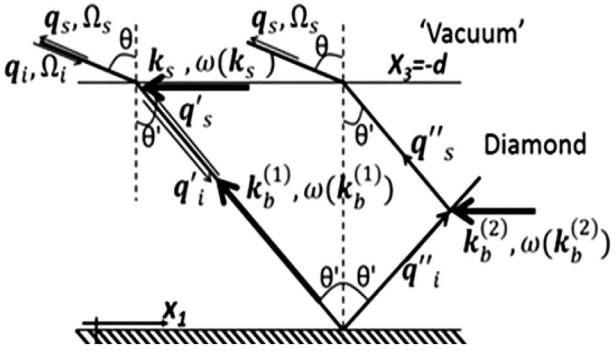

Fig. 7. Scattering geometry which best represents a transparent sample like diamond. Optical wavevectors are represented by thin arrow lines while thick arrows show acoustic wavevectors of bulk ($\boldsymbol{k}_b$) and surface ($\boldsymbol{k}_s$) acoustic waves. Ω_i, Ω_s are the incident and scattered optical angular frequencies; ω is the acoustical angular frequency; q_s, q_s are the incident and scattered optical wave vectors in 'vacuum'; $\boldsymbol{q}_i'$, $\boldsymbol{q}_s'$, $\boldsymbol{q}_i''$, $\boldsymbol{q}_s''$ are the incident and reflected optical wave vectors inside the medium before and after reflection, respectively, θ is the incident and scattering angles of the optical wave vector in 'vacuum' while θ' is the refracted and reflected angles of the acoustical wave vector at the sample holder [20].

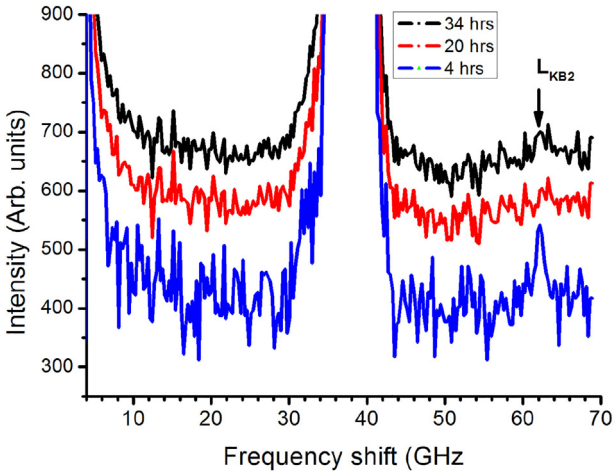

Fig. 8. Representative SBS spectra collected at the front of a 160 keV CIRA treated sample, showing cumulative acquiring up to 34 h, showing indirectly scattered L_{KB2} mode at ≈61.6 GHz.

Beghi *et al* [20] assert that in indirect backscattering (also called 2αA and only applicable to transparent materials), bulk acoustic modes are probed if the geometric wavelength (λ') is shorter than the film thickness. If however, the film thickness is smaller than the geometric wavelength of the probing light, other surface waves like Sezawa waves may be observed. In this section, where it is intended to get light reflect off the deep-seated 'mirror' and back through the diamond, the geometric wavelength of the layer would be important. In such a configuration the geometric wavelength $\lambda' = \lambda_o/2 \sin\theta$, is independent of the refractive index of the transparent film. Thus for angles of incidence that vary between 30° and 80°, the film thickness needs to be greater than 514.5 nm and 261.2 nm respectively, to observe the bulk waves due to indirect scattering. The bulk waves were observed in 0.3–0.5 mm thick samples as reported by Motochi *et al* [19]. Similarly, Beghi et al [20] studying bulk silica (2 mm thick) and thin silica film (2 μm thick) were able to observe a weak Rayleigh peak in bulk silica using backscattering (2αA) geometry but they do not report observing it in the forward (90R) or transmission (90A/platelet) geometries on the bulk or thin film samples. In their large samples they were able to observe the bulk modes (transverse and longitudinal). Therefore, probing a thin transparent diamond on a reflective opaque layer using the backscattering (2αA) geometry in this work was appropriate. Using P2 sample implanted at 160 keV, the large scattering volume at the back of the layer easily yields the bulk modes as shown in Fig. 9. When the same sample is turned so that light impinges from the front (small scattering volume), no obvious peaks were observed. Pronounced longitudinal modes from the back of the layer were observed L_{KB2} at 64.2 GHz while similar modes from the front L_{KB2} at 61.6 GHz were observed for laser beam $\lambda = 514.5$ incident at $\theta_i = 70°$ to the sample surface's normal. The difference is due to strain in the diamond film above the amorphous layer. This corroborates the results of the Raman measurement in Section 3.2 where the diamond signal was observed around 1326/1327 cm^{-1} instead of the Raman shift characteristic value for diamond, 1332 cm^{-1} [21].

The 'wipe-out' phenomenon was attributed to multiple reflections leading to what can be perceived as multiple sources of coherent inelastically scattered light being detected. Interference effects by division of the light would be expected when light is incident at an angle on such surfaces (two reflecting surfaces). In this scenario, part of the light is reflected from the top surface and the other is reflected at the interface. When these reflected beams overlap, interference effects (contour fringes) are observed due to the path difference traveled by light in the thin layer as shown in Fig. 6, the optical path difference is $2nt\ cos\ \theta$, where n is the refractive index of the medium between the reflecting

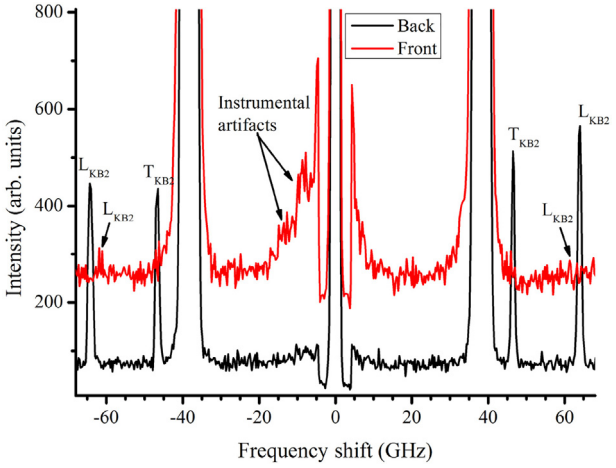

Fig. 9. SBS spectra collected at the front and back of a P2, 160 keV room temperature He ion implanted sample. There were small peaks, L_{KB2} at 61.6 GHz observed for the measurements from the front (red spectra), compared to measurement from the back (black spectra) that yielded pronounced indirectly scattered peaks T_{KB2} at 46.5 GHz and L_{KB2} at 64.2 GHz for laser beam $\lambda = 514.5$ incident at $\theta_i = 70^\circ$ to the sample surface's normal. (For interpretation of the references to colour in this figure legend, the reader is referred to the web version of this article.)

surfaces, t is the thickness of the layer and θ is the angle made with the normal by the light path in the medium. The approximate intensity of light detected due to multiple reflections between ≈100% reflective "surfaces" is calculated in Section 3.3.1. From these calculations the ideal calculated total reflectivity was 37% but this could be much less owing to absorption of the layer on the implanted side. Which explains the long time scales required for accumulation of photons scattering off the phonons to yield the indirect scattered peaks that later undergo a 'wipe-out' effect.

4. Conclusion

This work sought to study bulk modes on recrystallized diamond after implanting with He^+ and annealing at 1200 °C. The Raman and diffuse reflectance measurements show a recrystallized diamond film that forms a cap on the buried graphitic region. The diamond signal from the cap was observed around 1326/1327 cm^{-1} instead of the Raman shift characteristic value for diamond which is always observed at 1332 cm^{-1} implying that the recrystallized diamond was strained. The thin recrystallized diamond layer was estimated to be ≈103 nm for implantation at 160 keV using the constant angle reflection interference spectroscopy. SBS measurements on this cap produced weak modes T_{KB2} at 42.2 GHz and L_{KB2} at 61.6 GHz for laser beam $\lambda = 514.5$ incident at $\theta_i = 70^\circ$ to the sample surface's normal. However, the peaks suffered from 'wipe-out' effect. The 'wipe-out' was attributed to multiple scattering and interference effects arising from light reflecting off the diamond surface the diamond-graphitic interface buried below the thin diamond cap.

The support of the DST-NRF Centre of Excellence in Strong Materials (CoE-SM) towards this research is hereby acknowledged. Opinions expressed and conclusions arrived at, are those of the author and are not necessarily to be attributed to the CoE-SM. Special thanks to Dr. R. M. Erasmus for useful consultations and for the Raman spectroscopy measurements.

Author contribution

I Motochi: Conceptualization, Methodology, Investigation, Formal Analysis, Writing original draft.

E. Aradi: Formal Analysis, Validation, Writing-Review and editing.

B. A. Mathe: Conceptualization, Supervision, Methodology.

S.R. Naidoo: Conceptualization, Resources, Writing-Review and editing, Supervision, Funding acquisition.

Declaration of competing interest

There is no conflict of interest between the author and the funder.

References

[1] R.A. Spits, T.E. Derry, J.F. Prins, Annealing studies in ion implanted diamond, Nucl Instr. and Meth. B 64 (1992) 210–214.
[2] J.F. Ziegler, J.P. Biersack, M.D. Ziegler, The Stopping and Range of Ions in Matter, Publisher SRIM Co., Chester, Maryland, 2008 pages, 2-1.
[3] D.P. Hickey, K.S. Jones, R.G. Elliman, Amorphization and graphitization of single crystal diamond -a transmission electron microscopy study, Diam. Relat. Mat. 18 (2009) 1353–1359.
[4] J.O. Orwa, K.W. Nugent, D.N. Jamieson, S. Prawer, Raman investigation of damage by deep ion implantation in diamond, Phys. Rev. B 62 (2000) 5461–5472.
[5] T.E. Derry, E.K. Nshingabigwi, M. Levitt, J. Neethling, S.R. Naidoo, Cross-section transmission electron microscopy of the ion implantation damage in annealed diamond, Nucl. Instr. and Meth. B 267 (2009) 2705–2707.
[6] I. Motochi, S.R. Naidoo, B.A. Mathe, R. Erasmus, E. Aradi, T.E. Derry, E.J. Olivier, Surface Brillouin scattering on annealed ion-implanted CVD diamond, Diam. Relat. Mat. 56 (2015) 6–12.
[7] J.F. Prins, T.E. Derry, Cross-section transmission electron microscopy of the ion implantation damage in annealed diamond, Nucl. Instr. and Meth. in Phys. Res. B 166-167 (2000) 364–373.
[8] I. Motochi, B.A. Mathe, S.R. Naidoo, D. Wamwangi, T.E. Derry, Surface Brillouin scattering observation of higher order resonances in annealed, ion-implanted CVD diamond, Diam. Relat. Mat. 76 (2017) 171–176.
[9] C. Uzan-Saguy, C. Cytermann, R. Brener, V. Richter, M. Shaanan, R. Kalish, Damage threshold for ion-beam induced graphitization of diamond, Appl. Phys. Lett. 67 (1995) 1194–1196.
[10] A.V. Khomich, R.A. Khmelnitskii, V.A. Dravin, A.A. Gippius, E.V. Zavedeevand, I.I. Vlasov, Radiation damage in diamond subjected to helium implantation, Appl. Phys. Solid. Stat. 49 (2006) 1661–1665.
[11] A.C. Ferrari, J. Robertson, Resonant Raman spectroscopy of disordered, amorphous, and diamondlike carbon, Phys. Rev. B 64 (2001) 075414-1.
[12] Ingrid De Wolf, Micro-Raman spectroscopy to study local mechanical stress in silicon integrated circuits, Semicond. Sci. Technol. 11 (1996) 139–154.
[13] A.M. Goodman, Optical intereference method for the approximate determination of refractive index and thickness of a transparent layer, Appl. Optics 17 (1978) 2779–2787.
[14] M. Born, E. Wolf, 7th Ed. (Ed.), Principles of Optics: Electromagnetic Theory of Propagation, Interference and Diffraction of Light, 2003, pp. 317–319.
[15] G. Turri, S. Webster, Y. Chen, B. Wickham, A. Bennet, M. Bass, Index of refraction from near ultra-violet to the near-infrared from single crystal microwave assisted CVD diamond, Optical Mat. Express 7 (3) (2017) 855–859.
[16] D.W. Wheeler, R.J.K. Wood, Erosive wear behaviour of thick CVD diamond coatings, Wear 225-229 (1999) 523–536.
[17] B.J. Stagg, T.T. Charalampopoulos, Refractive indices of pyrolytic graphite, amorphous carbon, and flame soot in tempearture range 25 °C to 600 °C, Combusition and Flame. 94 (1993) 381–396.
[18] C. Sumanya, J.D. Comins, A.G. Every, Surface Brillouin scattering in opaque thin films, J. Phys.:Conference Series 92 (2007) 012103.
[19] I. Motochi, B.A. Mathe, S.R. Naidoo, T.E. Derry, Surface Brillouin scattering in ion-implanted chemical vapor deposited diamond, Mat. Today: Conference Proceedings 3S (2016) S145–S152.
[20] M.G. Beghi, F. Di Fonzo, S. Pietralunga, C. Ubaldi, C.E. Bottani, Precision and accuracy in film stiffness measurements by brillouin spectroscopy, Rev. Sci. Instrum. 82 (2011) 0533107-(1-11).
[21] A. Dychalska, P. Popielarsrski, W. Frankow, K. Fabisiak, K. Parprocki, M. Szybowicz, Study of CVD diamond layers with amorphous carbon admixture by Raman scattering spectroscopy, Mat. Sci. Poland. 334 (2015) 799–805.